Fabrication of Nickel NanoChains/PVDF Nanocomposites and Their Electrical/Magnetic Properties

Baptiste Martin, Eric Dantras, Antoine Lonjon, Lydia Laffont, Colette Lacabanne

Fabrication of Nickel NanoChains/PVDF Nanocomposites and Their Electrical/Magnetic Properties

Baptiste Martin, Eric Dantras, Antoine Lonjon, Lydia Laffont, and Colette Lacabanne*

Magnetic nickel nanoparticles (NPs) and nanochains (NNCs) are grown in a polyol medium under a static field as an alternative to template electrodeposition and strong reducers. Scanning electron microscopy (SEM) images and their statistical analysis show an important aspect ratio of 75 for NNCs. These NNCs present enhanced magnetic properties in terms of coercive field ($H_C = 163$ Oe) and saturation magnetization ($M_S = 10.8\,\text{emu}\,\text{g}^{-1}$). Nanocomposites of NNCs/PVDF are fabricated with 2 %vol. NNCs and present better properties than NPs/PVDF with higher filler content. The longitudinal and transverse magnetic properties of the composite are measured showing that higher properties are recorded in the longitudinal direction. Electrical conductivity of composite is plotted as a function of NNCs volume content to determine the electrical percolation threshold. The corresponding value of the apparent aspect ratio ($\xi = 70$) confirms that the processing of composite does not modify the particles morphology. Thus, it explains the enhancement of the magnetic properties due to the NNCs anisotropy.

1. Introduction

For the past 10 years, many studies have shown that the dispersion of ferromagnetic fillers in a diamagnetic matrix gave significant ferromagnetic properties.[1–3] Especially magnetic nano fillers present exceptional properties such as strong magnetization and high coercive field (H_c). Among them, nickel particles have received much attention due to several applications such as magnets, electronics, catalysis, or hyperthermia. Thanks to nanometer size, nickel can reach values of remnant magnetization (M_r) and coercive field (H_C) higher than bulk. However, at the nanometer scale, magnetic properties are strongly dependent on morphological aspects: that is, size, shape, and dimensionality.[4] To enhance these properties, the most interesting structure is the one dimensional one, with high aspect ratio.[5] Then, it is relevant to elaborate polymer based composites to enhance both the processability and magnetic characteristics of the material. Thus, it becomes possible with a low level of filler content to reach interesting magnetic properties and to preserve the polymer properties such as resilience in the same time. There are several ways of producing anisotropic nickel particles, like soft chemistry by growing particles together,[6] sol–gel synthesis,[7] or a solid-template route in porous anodic aluminum oxide (AAO) that permits to obtain good results for mono-crystalline and high aspect ratio.[8,9] However, this method requires a complex set up and it is not suitable for a large scale production. Since the first metallic particles obtained by Fievet et al.,[10] polyol process has shown its ability for larger production. Modified polyol routes have led to many particles shapes such as dumbbells,[11] rods,[12] fibers,[13] and wires.[14] Nickel nanochains (NNCs) growth has also been reported by using hydrazine as strong reducing agent in polyol under high magnetic field[14–20] without any chemical surfactant. The as-prepared particles show an important aspect ratio.

The aim of this work is to prepare high aspect-ratio nickel nanoparticles by a polyol route without employing any strong reducer or surfactant. A moderate unidirectional static magnetic field is applied during the reduction of nickel in polyol to orient the particles growth. The influence of external magnetic field intensity over the particles morphology is studied. Magnetic properties were also measured to study the influence of the raw particles morphology.

Once particles obtained, poly(vinylidene fluoride) (PVDF) based nanocomposites are processed to get flexible magnetic composites with enhanced properties. PVDF has been widely used as polymeric matrix in many applications such as energy harvesting materials,[21] sensors,[22] bioengineering,[23] and magnetoelectricity.[24] Like polymers PVDF is a diamagnetic material, so it will be interesting to introduce nickel to elaborate a flexible ferromagnetic composite. Due to NNCs anisotropic shape, the magnetic properties of NNCs/PVDF nanocomposites have been analyzed in transversal and longitudinal orientations. The introduction of conductive particles in polymers lead to conductive composites above percolation threshold as it was shown by the literature.[8,25–28] Consequently, the analysis of the electrical conductivity as a function of the NNCs volume content in PVDF

B. Martin, Dr. E. Dantras, Dr. A. Lonjon, Prof. C. Lacabanne
CIRIMAT
Physique des Polymères
Université de Toulouse
118 route de Narbonne, 31062 Toulouse Cedex 09, France
E-mail: eric.dantras@univ-tlse3.fr
Dr. L. Laffont
CIRIMAT
ENSIACET
Université de Toulouse
4 allée Emile Monso, CS44362, Toulouse 31030, France

DOI: 10.1002/pssa.201900158

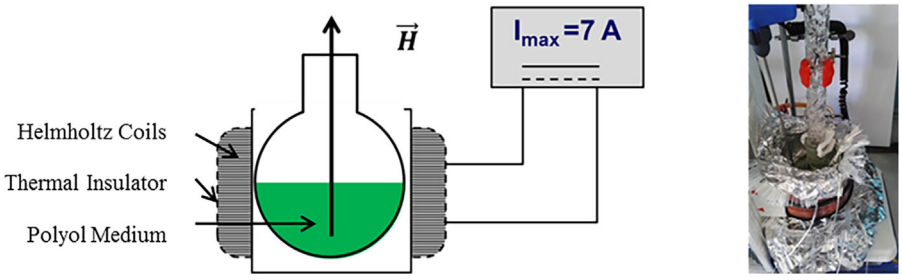

Figure 1. a) Schematic configuration of the magnetic-growth disposal and b) picture of the magnetic-growth disposal.

nanocomposites has been used to check the NNC aspect ratio after processing.

2. Experimental Section

2.1. Materials

PVDF powder was Kynar 500 (Arkema). Acetone is used as solvent for the polymer matrix and was purchased from Aldrich. Nickel Nanochains were reduced in 1.2 butanediol under a magnetic field by a method described in the following section.

2.2. Polyol Reduction of Nickel Nano Chains (NNC)

Chemicals are provided by Sigma–Aldrich. In a typical experimental procedure nickel acetate tetra hydrate (1 g) is dissolved in 1.2-butanediol (50 mL) under vigorous magnetic stirring until obtaining a strong green color. A nucleating solution is prepared by solving hydrated ruthenium chloride (1.10^{-3} mol) in 1.2-butanediol (100 mL). Five milliliters of this solution are introduced in the cold nickel solution. Finally, $NaOH_{(aq)}$ (2.10^{-3} mol) is added. The obtained solution is stirred under vigorous magnetic agitation for 30 min at 323 K. The mixture is then put in a round-bottomed-flask at 453 K for 20 min under a continuous and unidirectional magnetic field. When the temperature rose up to 453 K, the solution turns to black. The particles were obtained after 20 min then washed with distilled-water, ethanol, and acetone several times. The next step is to disperse the bundle of particles under sonication in ethanol. Once the particles are dispersed, the washing protocol is applied a second time to ensure that the entire polyol residues are gone.

The external magnetic field is provided by Helmholtz coils surrounding the reaction medium (**Figure 1**). They are powered by DC current to produce a unidirectional static and continuous magnetic field (between 0 and 10 mT) in the reaction medium. According to the applied magnetic field intensity we obtain pseudo spherical particles (NPs) or nickel nanochains (NNCs). The coils are isolated from the hot plate by a glass-fiber layer to keep them from thermal degradation.

The hot plate is nonmagnetic to avoid field perturbation and accidentally induced precipitation of the produced particles.

2.3. Nanocomposites Processing

The Poly (VinylyDene Fluoride) (PVDF) is dissolved in acetone at 348 K under stirring. Once the dissolution is completed, NNCs are dispersed in acetone by sonication. The solvent has been evaporated and the composite has been hot pressed (503 K) under 1 MPa to obtain a 200 µm thick film. Thermogravimetric analyses have been carried out and did not show any remaining solvent. Composites samples were obtained by cryo-cutting (fractography at liquid nitrogen temperature). The slice was deposed on carbon tape. SEM cryocut image (**Figure 2**) shows the homogeneous dispersion of particles in matrix. It also shows that the NNCs keep their aspect ratio.

2.4. Morphology and Surface Analyses

Samples morphology was determined using a JEOL 7800 Prime field emission scanning electron microscope (FE-SEM) operating at an accelerating voltage of 5 kV. To analyze precisely the Nickel nanotexture, bright field and high resolution images were performed using a JEOL JEM 2100F electron microscope operated at 200 kV and equipped of Energy Dispersive X-Ray Spectroscopy. Diffraction patterns were recorded using fast Fourier transform (FFT) of the HRTEM images.

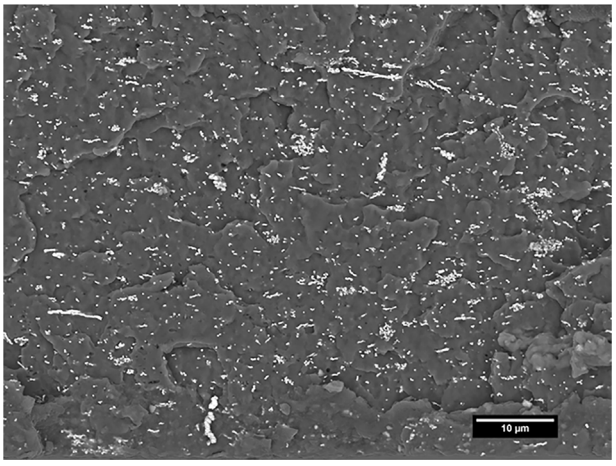

Figure 2. SEM cryocut image of a nanocomposite PVDF-NNCs 2 %vol.

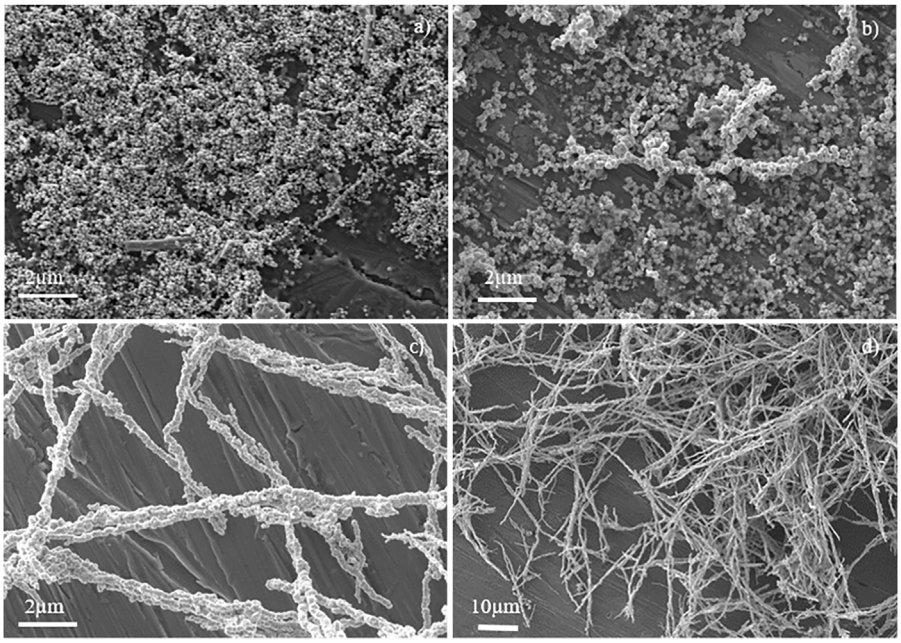

Figure 3. SEM images of obtained nickel particles at different magnetic fields: a) 0 mT; b) 5 mT; c) and d) 10 mT.

2.5. Magnetic Properties Measurement

The thermogravimetric analyzer (TGA) set up was used to determine the particles Curie temperature (T_c). A permanent magnet was put under the sample during the temperature ramp. When the temperature rises above Curie temperature (T_c) magnetic attraction vanishes leading to mass variation. T_c is taken at the endset point of this variation.

Magnetic properties – saturation magnetization (M_s), remaining magnetization (M_r), and coercive field (H_c) – were measured with a Superconducting Quantum Interference Device magnometer (SQUID). These measurements were carried out at four temperatures 2, 100, 300, and 400 K as a function of the applied field to plot the magnetic hysteresis cycle of the different samples.

2.6. Measurement of Electrical Properties

Samples have been coated with silver paint to improve the electrical contact with electrodes. All the conductivity measurements were carried out at room temperature. Low values of conductivity were determined by recording their complex conductivity $\sigma^*(\omega)$ on a Novocontrol broadband spectrometer between 10^{-2} and 10^6 Hz. The value of $\sigma'(\omega)$ at 10^{-2} is taken as the DC conductivity according to the analysis of Barrau et al.[24] High electrical conductivity values were measured on a Keithley 2420 Source Meter with a four-point probe configuration.

3. Results and Discussion

3.1. Electron Microscopies Analysis

The aim is to obtain Nickel nanochains at low magnetic field with a strong reproducibility. Ung et al.[11,29] showed in a previous work that reducing Ni and Co in 1.2-butanediol lead to anisotropic particles. In this study we use the same molar concentration of Ni^{2+} in liquid polyol. The hydroxyl ions concentration was also fixed at 0.2 M.

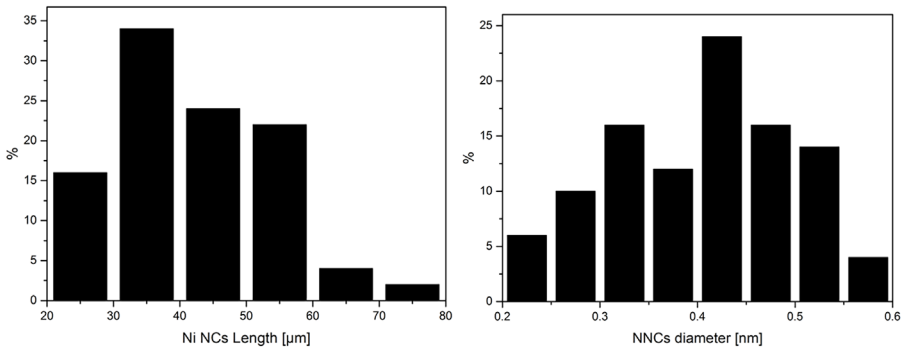

Figure 4. NNCs size distribution histogram of NNCs length and diameter from SEM statistical measurements.

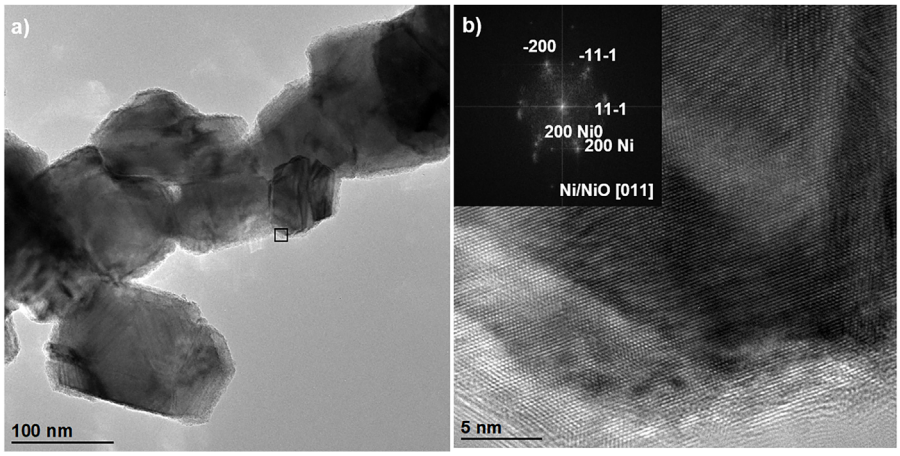

Figure 5. a) TEM and b) HRTEM images of NNCs in insert the FFT of the HRTEM image.

Heterogeneous nucleation has been used. It allows us to fix the number of particles by the introduction of a given amount of crystalline seeds. Furthermore, it makes the reaction time short enough to avoid homogeneous nucleation. A first reduction of Ni ions is lead without any external field (NPs@0mT). SEM picture shows spherical particles (**Figure 3**a) as reported previously by Fievet et al.[30] Then, we applied a 5 mT field looking for growth orientation. These particles (NPs@5mT) may show a slight orientation (Figure 3b) nevertheless they do not appear as anisotropic particles. The field was then raised up to 10 mT. Here a change has clearly been observed. The field is strong enough to have an incidence on the growth orientation, which lead to the formation of Nickel Nanochains (NNCs). Indeed, SEM analysis has shown an anisotropic shape with an important aspect ratio (Figure 3c and d). We also notice that our NNCs present a similar morphology as the ones obtained using hydrazine.[31] It means that method, reported in this work, is as efficient as hydrazine one. It presents a good alternative with soft reductant and short reaction time.

A statistical analysis is carried out on the SEM images (**Figure 4**) on one hundred particles. The particles exhibit a mean diameter of 400 nm and a mean length of about 30 µm. We estimate a mean aspect ratio labeled ξ with Equation (1) of 75.

$$\xi = \text{length}/\text{diameter} \quad (1)$$

TEM and HRTEM images (**Figure 5**a and b) show that the NNCs are made by a stacking of pseudo-spherical particles. It is important to note that these particles were sonicated and remained as NNCs. Furthermore, TEM study displays strong boundaries between the stacked-particles despite a weaker external magnetic field compared with Soumarre et al.[32] which report weak boundaries for a 0.7 T field. These results can be explained by a higher amount of hydroxyl ions (0.36 mol^{-1} against 0.15 mol^{-1}). Fast Fourier transform (FFT) of the HRTEM image (Figure 5b insert) shows the presence of a thin layer of NiO over the NNCs. This superficial oxidation can be assigned to the washing process of NNCs which implies water and drying in

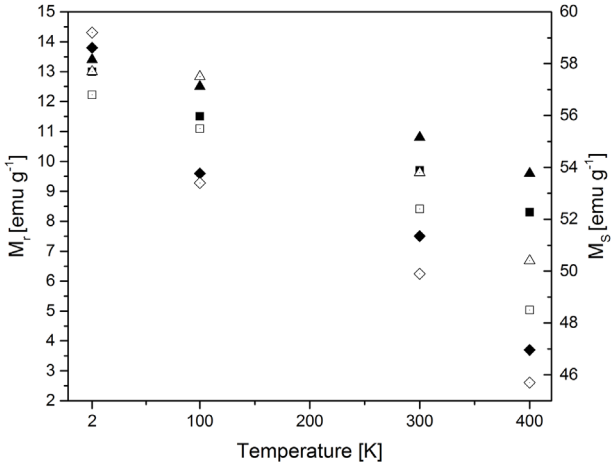

Figure 6. Nickel particles magnetization Mr (full symbols) and Ms (open symbols) as a function of temperature for the external field of ●NPs@0 mT, ■NPs@5 mT, and ▲NNCs@10 mT.

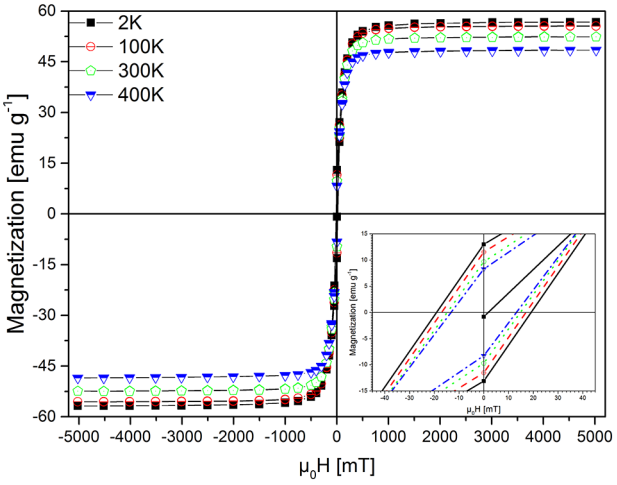

Figure 7. a) Magnetic hysteresis cycle at several temperatures for the 0 mT particles Insert: zoom between −50 and 50 mT.

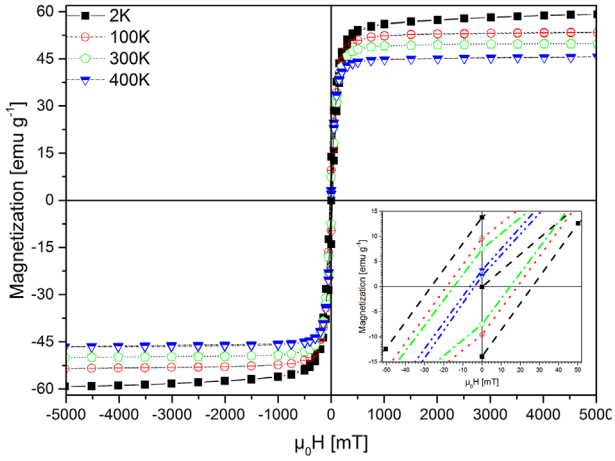

Figure 8. a) Magnetic hysteresis cycle at several temperatures for the 5 mT Ni particles. Insert: zoom between −50 and 50 mT.

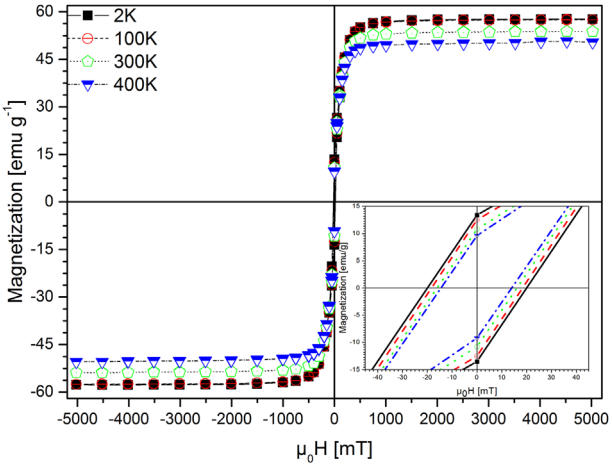

Figure 9. a) Magnetic hysteresis cycle at several temperatures for the NNCs. Insert: zoom between −50 and 50 mT.

oven at 353 K. FFT also confirms the good crystallinity of the NNCs particles.

3.2. Static Magnetic Properties of Ni Nanoparticles

Curie temperature (T_C) has been determined thanks to the TGA setup and the value taken at the curve endset. The measured value of 631.15 K, for each type of particle, including NNCs, shows a good agreement with the expected bulk Ni Curie temperature.[33] T_C does not depend on aspect ratio. Magnetic properties were determinate by SQUID. **Figure 6** shows the influence of temperature on magnetic moment alignment. As the temperature increases, magnetization decreases independently from their morphologies. In this work, we present the magnetic parameters values for the elaborated particles under 0 mT (**Figure 7**), 5 mT (**Figure 8**), and 10 mT (**Figure 9**) at four temperatures 2, 100, 300, and 400 K.

Regardless of the particle morphology the saturation magnetization (M_s) of particles at low temperatures (2 and 100 K) are very close to theoretical magnetic saturation of bulk Nickel (58.58 emu g^{-1}). At such temperatures thermal agitation is very low, so it allows an easy alignment of the magnetic moments along the magnetic field. The good agreement between the bulk Ni M_s and the obtained particles shows that the crystallinity of our particles is in agreement with nickel bulk crystal structure. It also underlines that the previously observed oxidation of the NNCs is very superficial and do not influence the magnetic properties.

Remnant magnetization (M_r) shows the same evolution with temperature as M_s. Independently from particle shape, M_r is about 13 emu g^{-1} and about 23% of M_s. Here the value of this ratio decreases with temperature due to thermal agitation (Figure 6). It confirms that the particles morphology does not change the M_s values at any temperature; the magnetization is an intrinsic value of the material, depending only on temperature and magnetic moments organization.

The random orientation of the powder in the measurement cell does not allow us to confirm an effect of the shape anisotropy over the coercive field (**Table 1**). It was previously reported that oriented NNCs shows higher M_r/M_s values. Nevertheless, we can notice that even isotropic particles already present enhanced magnetic properties over bulk Ni. The coercive field values also show a good agreement with previously reported results for this obtained particles without any magnetic field.[34]

Despite the random orientation, NNCs show a slightly higher H_c than spherical particles. It could be due to the shape anisotropy over the magnetic properties. It has been shown that a larger diameter induces a lower coercivity in this particle family.[30] In this work, the obtained particles exhibit a mean diameter of 400 nm which explain, in addition with the random orientation, the lower H_c values for the NNCs as the one reported by Soumare.[32]

The M_r and H_c values are 10.8 emu g^{-1} and 163 Oe at 300 K, respectively (Table 1). These values are consistent with the NNCs reduced by hydrazine,[18,19,35] showing that our system is a good alternative to these strong reducing systems. These values are also in the same order of magnitude as the magnetic properties of the electro-deposed nickel nanowires.[36]

3.3. Magnetic Properties of the NNCs/PVDF Composites

The NNCs content was fixed at 2 vol% to preserve as much as possible the polymer mechanical properties. Magnetization was measured along the polymer surface and through it.

The magnetization curves at ambient temperature (**Figure 10**) show a ferromagnetic behaviour despite the low filler content with a coercivity of 180 Oe perpendicularly to the composite plane and 210 Oe along the composite plane. The M_s at 5 T is 3.8 emu g^{-1} in

Table 1. Magnetic properties for the different particles at 300 K.

	M_s [emu g^{-1}]	M_r [emu g^{-1}]	M_r/M_s	H_c [Oe]
NPs @0mT	58	9.7	18	148
NPs @5mT	58	8.7	15	63
NNCs	58	10.8	20	163

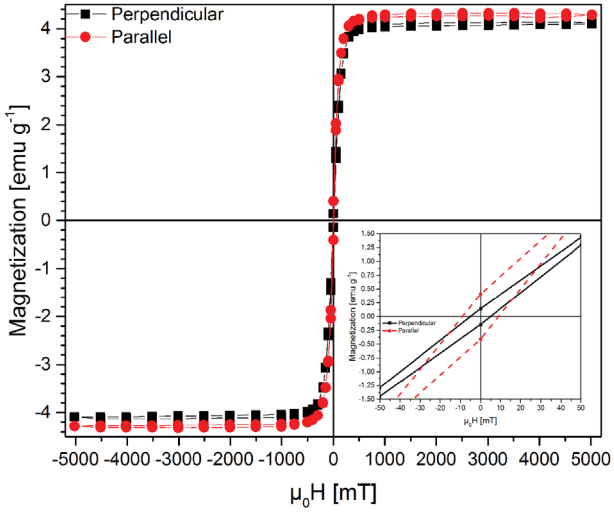

Figure 10. Parallel and perpendicular magnetization of a 2 vol %. NNCs-PVDF nanocomposite at 300 K. Insert: zoom between −50 and 50 mT.

both directions. M_r show important differences depending on the orientation with a longitudinal value of 0.41 emu $g^{-1}$and a transverse value of 0.14 emu g^{-1}. This difference is explained by the composite processing which leads to an orientation of the NNCs. This effect is combined with the shape anisotropy of NNCs leading to an easier magnetic orientation along the composite. The values of H_c are consistent with the previous results obtained for raw NNCs and in the same order of magnitude than a 5 %vol NNCs/PVDF composite.[37] The lower M_r value was expected because of the large amount of PVDF in composite but remains high in comparison with the amount of magnetic phase. Literature provides such values for ferrites composites[37,38,39] but for much higher filler content. Furthermore, the aspect ratio of NNCs enhanced the magnetic properties of Ni/PVDF composite leading to higher values of magnetization than a 10% weight spherical particles composite.[40,41]

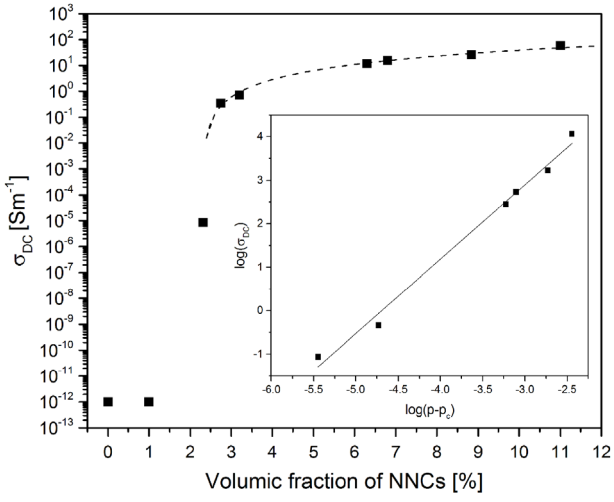

Figure 11. Transverse conductivity as a function of the NNCs volume fraction; the dotted line corresponds to Equation (2). Insert: Fit by the power law of the dotted line.

3.4. Electrical Conductivity of NNCs/PVDF Composites

Dispersing conductive particles in a dielectric matrix can lead to a critical phenomenon called percolation. This phenomenon depends mainly on the particle aspect ratio ξ defined by Equation (1). The transverse conductivity σ_{DC} of composites is reported as a function of the NNCs volume fraction in the NNCs/PVDF composite at room temperature to determinate the percolation threshold value (**Figure 11**). At low volume fraction, the conductivity shows a value close to matrix conductivity. When the fraction reached 2.5 %vol the conductivity increase by 13 decades from 10^{-12} to 50 S m^{-1}. This phenomenon is the manifestation of the electrical percolation path formation allowing the electrons transport across the composite. The electrical conductivity raises up to 50 S m^{-1} at 8 %vol which is slightly lower than value obtain with electro-deposed metal nanowires.[8,25] This decrease can be associated with the superficial oxidation observed on the TEM images. The conductivity values above the percolation threshold were fitted with the following power law (Equation 2):

$$\sigma = \sigma_0 \times (p - p_c)^t \quad (2)$$

where σ is the measured conductivity, σ_0 the theoretical value of 100% NNCs "composite," p and p_c the volume fraction and the percolation volume fraction respectively.

Figure 11 clearly shows an increase of DC conductivity linked to the percolation phenomenon. The experimental values are in a good agreement with the model shown in insert of Figure 11. The percolation threshold is found close to $p_c = 2.3\%$, $\sigma_0 = 3000$ S m^{-1}, and $t = 1.71$. The p_c value is higher as the one obtained for electro-deposed Ni NWs (0.75 %vol for an aspect ratio of 250[8]) due to a lower aspect ratio as shown in the literature.[42] σ_0 represent the theoretical conductivity of raw NNCS. Here σ_0 reaches a value of 3.10^3 S m^{-1}. This value is lower than the nickel bulk conductivity (1.4×10^7 S m^{-1}); that is, due to the NNCs surface oxidation. The critical exponent t is determined close to 1.7. The Kirpatrick law predict a 3D dispersion for a t value between $1.6 \leq t \leq 2$. Considering the random dispersion of rigid sticks and the fillers anisotropy, it is possible to link the exponent value to the exclude volume Balberg model[43]:

$$f_a \times p_c = 1.6 \pm 0.2 \quad (3)$$

where f_a is the apparent aspect ratio of the particles in the composite and p_c the percolation threshold in volume fraction leading to an apparent aspect ratio f_a of 70. This value is close to the value determined by SEM images analysis (cf Section 3.1). The slight decrease can be explained by the composite processing which might curve the nanowires.

4. Conclusion

Nickel nanochains were successfully obtained by a soft and modified polyol route without any further reducing agent and at atmospheric pressure by applying a 10 mT external continuous magnetic field during crystallogenesis. The statistical analysis gives an important aspect ratio of 75. HRTEM combined to FFT have shown a superficial oxidation leading to passivation of the

NNCs. The magnetic properties like remnant magnetisation M_r and coercive field H_c of NNCs are higher than for spherical particles but also for NNCs obtained with PVP and hydrazine. Thus, the proposed crystallogenesis procedure clearly appears as a good alternative for NNCs fabrication.

NNCs/PVDF composites have been successfully fabricated by precipitation and hot pressing. The longitudinal and transverse magnetic properties of a 2 %vol NNCs/PVDF composite have been measured showing that higher properties are recorded in the longitudinal direction. After the percolation threshold, the electrical conductivity is close to $50\,S\,m^{-1}$. Meanwhile, the percolation threshold has been determined at 2.3 %vol NNCs. It suits well to an aspect ratio of 70 for NNCs which is consistent with the value 75 deduced from the statistical analyses of SEM images of NNCs.

Conflict of Interest

The authors declare no conflict of interest.

Keywords

electrical percolation, magnetic properties, nickel nanochains, polyol synthesis, PVDF

[1] P. Martins, C. M. Costa, S. Lanceros-Mendez, *Appl. Phys. A* **2011**, *103*, 233.

[2] R. Gonçalves, P. Martins, D. M. Correia, V. Sencadas, J. L. Vilas, L. M. León, G. Botelho, S. Lanceros-Méndez, *RSC Adv.* **2015**, *5*, 35852.

[3] M. Petrychuk, V. Kovalenko, A. Pud, N. Ogurtsov, A. Gubin, *Phys. Status Solidi A* **2010**, *207*, 442.

[4] J. Zhang, X. Qin, B. Torre, H. Zeng, X. Xu, *IEEE Trans. Magn.* **2014**, *50*, 1.

[5] M. Vázquez, H. Chiriac, A. Zhukov, L. Panina, T. Uchiyama, *Phys. Status Solidi A* **2011**, *208*, 493.

[6] M. Yan, J. Fresnais, S. Sekar, J.-P. Chapel, J.-F. Berret, *ACS Appl. Mater. Interfaces* **2011**, *3*, 1049.

[7] M. Alagiri, C. Muthamizhchelvan, S. Ponnusamy, *Synth. Met.* **2011**, *161*, 1776.

[8] A. Lonjon, L. Laffont, P. Demont, E. Dantras, C. Lacabanne, *J. Phys. Chem. C* **2009**, *113*, 12002.

[9] J. García, V. Vega, L. Iglesias, V. M. Prida, B. Hernando, E. D. Barriga-Castro, R. Mendoza-Reséndez, C. Luna, D. Görlitz, K. Nielsch, *Phys. Status Solidi A* **2014**, *211*, 1041.

[10] F. Fievet, J. P. Lagier, B. Blin, B. Beaudoin, M. Figlarz, *Solid State Ion.* **1989**, *32*, 198.

[11] D. Ung, Y. Soumare, N. Chakroune, G. Viau, M.-J. Vaulay, V. Richard, F. Fiévet, *Chem. Mater.* **2007**, *19*, 2084.

[12] K. A. Atmane, F. Zighem, Y. Soumare, M. Ibrahim, R. Boubekri, T. Maurer, J. Margueritat, J.-Y. Piquemal, F. Ott, G. Chaboussant, *J. Solid State Chem.* **2013**, *197*, 297.

[13] C. Zhang, Y. Yao, J. Zhan, J. Wu, C. Li, *J. Phys. Appl. Phys.* **2013**, *46*, 495308.

[14] J. Zhang, W. Xiang, Y. Liu, M. Hu, K. Zhao, *Nanoscale Res. Lett.* **2016**, *11*, 118.

[15] W. Xu, Y.-F. Pan, W. Wei, G.-S. Wang, P. Qu, *Appl. Surf. Sci.* **2018**, *428*, 54.

[16] X. Ni, H. Zheng, Y. Shan, X. Cai, X. Jin, G. Liao, *J. Alloys Compd.* **2009**, *481*, 764.

[17] B. P. Mandal, K. Vasundhara, E. Abdelhamid, G. Lawes, H. G. Salunke, A. K. Tyagi, *J. Phys. Chem. C* **2014**, *118*, 20819.

[18] H. Wang, M. Li, X. Li, K. Xie, L. Liao, *Bull. Mater. Sci.* **2015**, *38*, 1285.

[19] J. Wang, L. Y. Zhang, P. Liu, T. M. Lan, J. Zhang, L. M. Wei, Y. F. Zhang, C. H. Jiang, *Nano-Micro Lett.* **2010**, *2*, 134.

[20] L. Sun, Q. Chen, *Eur. J. Inorg. Chem.* **2009**, *2009*, 435.

[21] H. Parangusan, D. Ponnamma, M. A. A. AlMaadeed, *Soft Matter* **2018**, *14*, 8803.

[22] D. Ponnamma, S. Goutham, K. K. Sadasivuni, K. V. Rao, J. J. Cabibihan, M. A. A. Al-Maadeed, *Synth. Met* **2018**, *243*, 34.

[23] H. Parangusan, D. Ponnamma, M. A. A. Al-Maadeed, *Sci. Rep.* **2018**, *8*, 754.

[24] P. Martins, S. Lanceros-Méndez, *Adv. Funct. Mater.* **2013**, *23*, 3371.

[25] A. Lonjon, L. Laffont, P. Demont, E. Dantras, C. Lacabanne, *J. Phys. Appl. Phys.* **2010**, *43*, 345401.

[26] L. Q. Cortes, A. Lonjon, E. Dantras, C. Lacabanne, *J. Non-Cryst. Solids* **2014**, *391*, 106.

[27] L. Rivière, A. Lonjon, E. Dantras, C. Lacabanne, P. Olivier, N. R. Gleizes, *Eur. Polym. J.* **2016**, *85*, 115.

[28] S. Barrau, P. Demont, A. Peigney, C. Laurent, C. Lacabanne, *Macromolecules* **2003**, *36*, 5187.

[29] D. Ung, G. Viau, C. Ricolleau, F. Warmont, P. Gredin, F. Fiévet, *Adv. Mater.* **2005**, *17*, 338.

[30] F. Fiévet, S. Ammar-Merah, R. Brayner, F. Chau, M. Giraud, F. Mammeri, J. Peron, J.-Y. Piquemal, L. Sicard, G. Viau, *Chem. Soc. Rev.* **2018**, *47*, 5187.

[31] S. Tang, S. Vongehr, H. Ren, X. Meng, *CrystEngComm* **2012**, *14*, 7209.

[32] Y. Soumare, A. Dakhlaoui-Omrani, F. Schoenstein, S. Mercone, G. Viau, N. Jouini, *Solid State Commun.* **2011**, *151*, 284.

[33] D. L. Connelly, J. S. Loomis, D. E. Mapother, *Phys. Rev. B* **1971**, *3*, 924.

[34] A. D. Omrani, M. A. Bousnina, L. S. Smiri, M. Taibi, P. Leone, F. Schoenstein, N. Jouini, *Mater. Chem. Phys.* **2010**, *123*, 821.

[35] J. Y. Liao, H. Li, J. J. Liang, Y. F. Feng, X. B. Zhang, Y. Q. Yin, H. X. Tao, *Nano* **2013**, *08*, 1350005.

[36] T. H. L. Nguyen, L. Laffont, J.-F. Capsal, P.-J. Cottinet, A. Lonjon, E. Dantras, C. Lacabanne, *Mater. Chem. Phys.* **2015**, *153*, 195.

[37] H. Denver, T. Heiman, E. Martin, A. Gupta, D.-A. Borca-Tasciuc, *J. Appl. Phys.* **2009**, *106*, 064909.

[38] C. Behera, R. N. P. Choudhary, P. R. Das, *J. Electron. Mater.* **2017**, *46*, 6009.

[39] H. Ranjan, U. K. Mahto, K. P. Chandra, A. R. Kulkarni, A. Prasad, K. Prasad, *J. Adv. Dielectr.* **2017**, *07*, 1750036.

[40] B. P. Mandal, K. Vasundhara, E. Abdelhamid, G. Lawes, H. G. Salunke, A. K. Tyagi, *J. Phys. Chem. C* **2014**, *118*, 20819.

[41] C. Sirisathitkul, P. Jantaratana, N. Muensit, *Sci. Eng. Compos. Mater.* **2012**, *19*, 255.

[42] A. Lonjon, P. Demont, E. Dantras, C. Lacabanne, *J. Non-Cryst. Solids* **2012**, *358*, 3074.

[43] I. Balberg, C. H. Anderson, S. Alexander, N. Wagner, *Phys. Rev. B* **1984**, *30*, 3933.